Advanced Robotics

ISSN: 0169-1864 (Print) 1568-5535 (Online) Journal homepage: https://www.tandfonline.com/loi/tadr20

Optimal Design of a 6-DOF Parallel Manipulator Using Particle Swarm Optimization

A.R. Shirazi , M.M.S. Fakhrabadi & A. Ghanbari

To cite this article: A.R. Shirazi , M.M.S. Fakhrabadi & A. Ghanbari (2012) Optimal Design of a 6-DOF Parallel Manipulator Using Particle Swarm Optimization, Advanced Robotics, 26:13, 1419-1441, DOI: 10.1080/01691864.2012.690187

To link to this article: https://doi.org/10.1080/01691864.2012.690187

Taylor & Francis
Taylor & Francis Group

Advanced Robotics 26 (2012) 1419–1441

ADVANCED ROBOTICS
tandfonline.com/tadr

Full paper

Optimal Design of a 6-DOF Parallel Manipulator Using Particle Swarm Optimization

A.R. Shirazi[a], M.M.S. Fakhrabadi[b]* and A. Ghanbari[a]

[a]Mechatronics Research Laboratory, School of Engineering, Emerging Technologies, University of Tabriz, 22 Bahman Blvd., P.O. Code: 51666-16471, Tabriz, Iran; [b]Karaj Branch, Islamic Azad University, Karaj, Iran

Received 19 August 2011; accepted 6 October 2011

Abstract

Performance indices of parallel manipulators (PMs) vary widely with the variation of geometric properties. Improvement of one parameter often leads to worsen the other parameters. Therefore, getting into an optimum design for the PMs has been subject of much recent research. In this paper, we optimize three performance parameters of a PM simultaneously including workspace, condition number, and stiffness. In addition, a new performance index is introduced for stiffness evaluation of the PMs. The index is invariant under similarities. Because of complexity of cost function and number of variables, choosing an optimization method that can converge to the optimum point is very important. We select particle swarm optimization (PSO) method and show that this algorithm is perfect for performance optimization of PMs. Furthermore, we propose a new subroutine added to PSO algorithm to improve its convergence.

Keywords

parallel robot, workspace, stiffness, condition number, multicriteria optimum design, particle swarm optimization

1. Introduction

Due to the advantages rather than series manipulators (SMs), some researchers have investigated parallel manipulators (PMs) in recent years (see, e.g. Refs [1–7]). PM is a robotic arm whose end effector (EE) connects to the base via at least two kinematic chains. In this way, the load applied on the EE is distributed on several chains. For this reason, PMs have more stiffness compared to SMs. In addition, more accuracy and possibility of achieving higher speeds for the EE are other advantages of the PMs (see, e.g. Ref. [8]). On the other hand, smaller workspace is the most serious disadvantage of PMs. In fact, to achieve more

* To whom correspondence should be addressed. E-mail: msfakhrabadi@gmail.com

 DOI: 10.1080/01691864.2012.690187

accuracy and stiffness, we have more constrained workspace. The purpose of this paper is to have an optimum design with high accuracy and stiffness and an acceptable workspace. A trade-off between these parameters is to be investigated here. Because the mentioned parameters highly depend on structural geometry of the robot, small variations in design variables can contribute to notable variations in the performance indices.

Many attempts have been made to optimize two or more performance parameters simultaneously. Kim and Tsai [9] optimized the stiffness of a Cartesian PM for a given workspace. They considered the average of stiffness on total of the workspace as stiffness parameter. Hao and Merlet [10] proposed a design approach with multicriteria requirement based on interval analysis. Lou et al. [11] studied a global approach to optimize multiple criteria performance characteristics. In this way, many parameters such as condition number, accuracy, stiffness, maximum velocity, and maximum force were reduced to constraints on singular values of the kinematics Jacobian matrix. Monsarrat and Gosselin [12] optimized singularity of free workspace of a three-legged 6-DOF parallel robot. In another research, Badescu and Mavroidis [13] optimized the workspace and condition number of a three-legged Universal-Prismatic-Universal (UPU) and Universal-Prismatic-Spherical (UPS) parallel platforms. They used a discretization method and discretized space to 1,000,000 points and then selected points randomly using Monte Carlo method and evaluated them. In addition, they considered joints constrains.

Reaching to an algebraic relationship between design variables and performance parameters and their optimization is very difficult using steepest descent or other methods based on derivations of the cost function. Here, the new optimization methods help. In recent works, genetic algorithm (GA) has been used

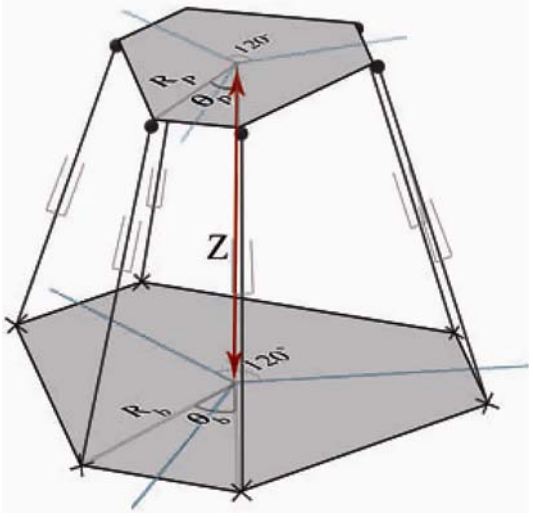

Figure 1. Structural geometry of PM under discussion.

to solve the optimization problems. For instance, Hwang et al. [14] optimized a 6-DOF PM for workspace, orientation, and global condition index using GA. Gao et al. [15] optimized a spatial 6-DOF PM using GA approach for workspace and condition number. Xu and Li [16] used three different approaches to optimize structural parameters of a class of translational PMs. The approaches were Nelder–Mead simplex (NMS) algorithm, GA, and particle swarm optimization (PSO). They compared the algorithms and then showed that the PSO method enjoyed a better convergence rate than NMS and GA procedures. In addition, it had no sensitivity to the initial conditions.

In this work, the method used to optimize PM is PSO. Kennedy, Eberhart, and Shi established PSO with simulation of the group lives of birds and fish in 1995 [17]. Many attempts have been made in recent years to improve on PSO. Trelea [18] evaluated parameter selection to improve the convergence of the algorithm. Jiang et al. [19] indicated that the positions of the particles can be considered in a stochastic vector form and analyzed the convergence of the algorithm. In another study, Teruyoshi [20] proposed an approach for self-tuning of the parameters of PSO. Similarly, we try to improve PSO and propose a new subroutine for this algorithm that helps its convergence to global minimum.

2. Kinematic Analysis

Because of the closed chain, kinematic analysis of PMs is partly complicated. Various methods have been developed for instantaneous kinematic analysis of PMs (see, e.g. Refs [21–24]).The method we use in this paper is the *screw theory*.

Screws assigned to joints of *i*th limb are shown in Fig. 2.

Spherical joints are considered as three revolute joints and universal joints as two revolute joints. Hence six screws of six joints are indicated as:

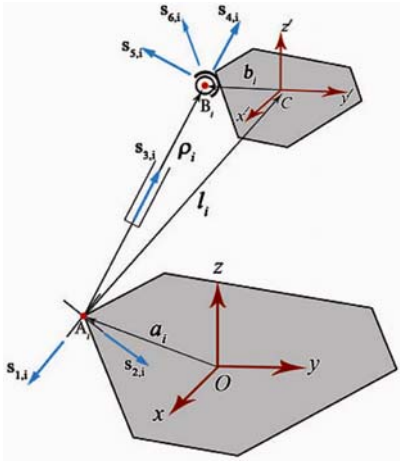

Figure 2. Screws assigned to the joints.

$$\hat{\$}_{\mathbf{1,i}} = \begin{bmatrix} \mathbf{s_{1,i}} \\ \mathbf{a_i} \times \mathbf{s_{1,}}_i \end{bmatrix}, \quad \hat{\$}_{\mathbf{2,i}} = \begin{bmatrix} \mathbf{s_{2,i}} \\ \mathbf{a_i} \times \mathbf{s_{2,}}_i \end{bmatrix}, \quad \hat{\$}_{\mathbf{3,i}} = \begin{bmatrix} \mathbf{0} \\ \mathbf{s_{3,}}_i \end{bmatrix},$$
$$\hat{\$}_{\mathbf{4,i}} = \begin{bmatrix} \mathbf{s_{4,i}} \\ (\mathbf{a_i} + \boldsymbol{\rho}_\mathbf{i}) \times \mathbf{s_{4,}}_i \end{bmatrix}, \quad \hat{\$}_{\mathbf{5,i}} = \begin{bmatrix} \mathbf{s_{5,i}} \\ (\mathbf{a_i} + \boldsymbol{\rho}_\mathbf{i}) \times \mathbf{s_{5,}}_i \end{bmatrix}, \tag{1}$$
$$\hat{\$}_{\mathbf{6,i}} = \begin{bmatrix} \mathbf{s_{6,i}} \\ (\mathbf{a_i} + \boldsymbol{\rho}_\mathbf{i}) \times \mathbf{s_{6,}}_i \end{bmatrix},$$

where

$$\mathbf{S_{1,}}_i = \begin{bmatrix} 1 \\ 0 \\ 0 \end{bmatrix}, \quad \mathbf{S_{3,}}_i = \mathbf{S_{4,}}_i = \frac{\boldsymbol{\rho}_\mathbf{i}}{|\boldsymbol{\rho}_\mathbf{i}|}, \quad \mathbf{S_{2,}}_i = \mathbf{S_{1,}}_i \times \mathbf{S_{3,}}_i, \quad \mathbf{S_{6,}}_i = \mathbf{S_{5,}}_i \times \mathbf{S_{4,}}_i.$$

The screw which is the reciprocal of all screws except $\hat{\$}_{\mathbf{3;i}}$ is represented by $\hat{\$}_{\mathbf{r,i}}$. With some investigation, we find that $\hat{\$}_{\mathbf{r;i}}$ is:

$$\hat{\$}_{\mathbf{r,i}} = \begin{bmatrix} \mathbf{s_{3,}}_i \\ \mathbf{a_i} \times \mathbf{s_{3,}}_i \end{bmatrix}. \tag{2}$$

Multiplying Equation (2) by both sides of Equation (1), we have:

$$\theta_{3,i} = [\mathbf{s_{3,i}}\ \mathbf{a_i} \times \mathbf{s_{3,i}}]\mathbf{S_t}. \tag{3}$$

Hence, ith row of inverse kinematics Jacobian matrix is represented as follows:

$$\mathbf{J}_{\alpha\mathbf{i}}^{-\mathbf{1}} = \begin{bmatrix} \dfrac{\boldsymbol{\rho}_\mathbf{i}}{|\boldsymbol{\rho}_\mathbf{i}|} & \mathbf{a_i} \times \dfrac{\boldsymbol{\rho}_\mathbf{i}}{|\boldsymbol{\rho}_\mathbf{i}|} \end{bmatrix}. \tag{4}$$

To evaluate this inverse Jacobian matrix, we choose the coordinate system of the base as reference coordinate system. Because of dependency of Jacobian matrix to choosing operating point, we should transfer the coordinate system to the operating point C.

According to Fig. 3, a transferred screw can be written as:

$$\$_\mathbf{t} = \begin{bmatrix} \mathbf{s} \\ \mathbf{s_0} \times \mathbf{s} - \mathbf{T} \times \mathbf{s} \end{bmatrix}. \tag{5}$$

The position vector of the operating point is $\mathbf{T}$. In this case, $\mathbf{T}$ is:

$$\mathbf{T} = \mathbf{a_i} + \mathbf{l_i}. \tag{6}$$

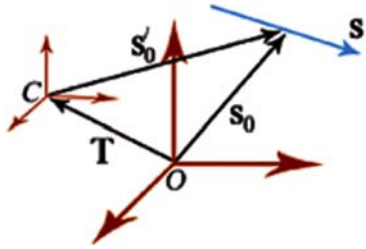

Figure 3. Transferring coordinate system to the operating point.

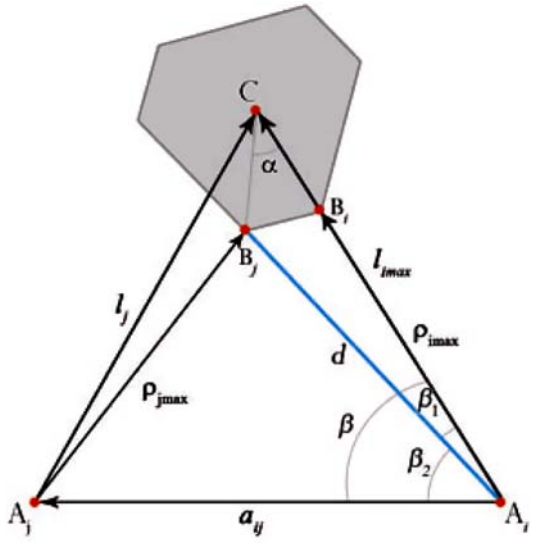

Figure 4. Evaluating the modified length.

Inverse of kinematics Jacobian matrix is obtained from Equations (4)–(6). Its *i*th row is:

$$\mathbf{J}_\mathbf{i}^{-1} = \left[\frac{\boldsymbol{\rho}_\mathbf{i}}{|\boldsymbol{\rho}_\mathbf{i}|} \qquad \frac{\boldsymbol{\rho}_\mathbf{i}}{|\boldsymbol{\rho}_\mathbf{i}|} \times \mathbf{l}_\mathbf{i} \right]. \tag{7}$$

3. Workspace

Many different algorithms have been developed to evaluate the workspace of PMs (see, e.g. Refs [25,26]). Gosslin [27] presented an algorithm to evaluate the workspace of a 6-DOF PM for a fixed orientation of the EE. To evaluate total workspace, we run algorithm for all orientations of the EE that is a very time-consuming process, not proper for use in optimization. Kim et al. [28] presented a fast algorithm to estimate total workspace of a 6-DOF PM with acceptable

approximations. Here, we explain and develop this algorithm in more detail to apply to our work. According to Fig. 4, the conjunction point of limb i and the base is represented by A_i and the point of conjunction of limb i and platform is represented by B_i. Therefore, $\boldsymbol{\rho}_i = \mathbf{B}_i - \mathbf{A}_i$ denotes the length and orientation of limb i and its magnitude varies between ρ_{min} and ρ_{min}. Point C is the center of the coordinate system located on platform. The region to which C can reach is defined as workspace. As shown in Fig. 4, $\mathbf{l}_i$ can be formulated as:

$$\mathbf{l}_i = \mathbf{C} - \mathbf{a}_i. \tag{8}$$

To estimate the workspace, we calculate minimum and maximum $\mathbf{l}_i$:

$$|\mathbf{l}_{i\max}| = \rho_{i\max} + R_P; \tag{9a}$$

$$|\mathbf{l}_{i\min}| = \rho_{i\min} - R_P. \tag{9b}$$

For each limb, these two spheres are defined as:

$$(\overline{\mathbf{OC}} - \mathbf{a}_i) \cdot (\overline{\mathbf{OC}} - \mathbf{a}_i) = \mathbf{l}_{i\max}; \tag{10a}$$

$$(\overline{\mathbf{OC}} - \mathbf{a}_i) \cdot (\overline{\mathbf{OC}} - \mathbf{a}_i) = \mathbf{l}_{i\min}. \tag{10b}$$

The reachable space for each limb is the space between the spheres. Total workspace of the robot roughly equals to intersections of the reachable workspaces of all limbs. We can obtain a better approximation using the concept of *modified length*. In this method, we calculate new lengths for $\mathbf{l}_{i\max}$ and $\mathbf{l}_{i\min}$. The new lengths are represented by $l_{i\max}^{\text{modified}}$ and $l_{i\min}^{\text{modified}}$.

The main idea to evaluate the length is that, when l_i has maximum magnitude, l_j belonging to jth limb cannot have maximum length because of keeping platform in rigid shape and maintaining geometric relations. In this state, the maximum length of l_j is less than $l_{j\max}$, that we represent it by $l_{j\max}^{\text{modified}}$.

According to Fig. 4, suppose that $A_i, A_j, B_i,$ and B_j are located on a same plane. The values l_i, ρ_i, and ρ_j have maximum lengths and are equal to $l_{i\max}$, $\rho_{i\max}$, and $\rho_{j\max}$, respectively.

Distance d is:

$$d = \sqrt{R_b^2 + l_{i\max}^2 - 2R_p l_{i\max}\cos\alpha}. \tag{11}$$

Then β_1 and β_2 can be written as:

$$\beta_1 = \cos^{-1}\left(\frac{d^2 + l_{i_{\max}}^2 - R_p^2}{2\mathrm{d}l_{i_{\max}}}\right); \tag{12a}$$

$$\beta_2 = \cos^{-1}\left(\frac{d^2 + a_{ij}^2 - \rho_{j_{\max}}^2}{2\mathrm{d}a_{ij}}\right). \tag{12b}$$

The angle β is:

$$\beta = \begin{cases} \beta_1 + \beta_2 & \alpha \leqslant 180 \\ \beta_2 + \beta_1 & \alpha > 180 \end{cases}. \tag{13}$$

Hence the modified length of limb j with respect to the limb i is:

$$l_{j\max}^{\text{modified}} = \sqrt{l_{i\max}^2 + a_{ij} - 2l_{i\max}a_{ij}\cos\beta}. \tag{14}$$

To compute $l_{j\min}^{\text{modified}}$, the equations are similar to the relations above, except that α, $\rho_{i\max}$, $\rho_{j\max}$, and $l_{i\max}$ should be replaced, respectively, by $(\alpha - 180)$, $\rho_{i\min}$, $\rho_{j\min}$, and $l_{i\min}$. The number of modified lengths is 15 cases for maximum and 15 cases for minimum lengths. With symmetry of structure, the cases are reduced to 9 for minimums and 9 for maxima. We select the minimum of modified maximum length and maximum of modified minimum length:

$$l'_{\max} = \min(l_{\max}^{\text{modified}}), \tag{15a}$$

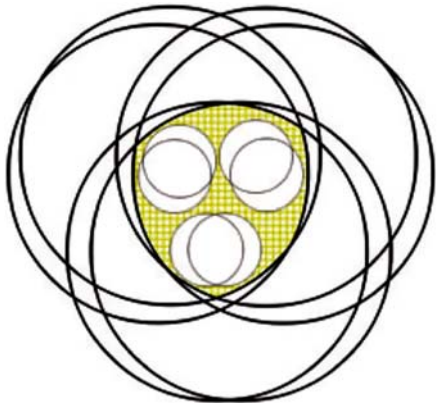

Figure 5. Twelve circles defining the cross-section of workspace.

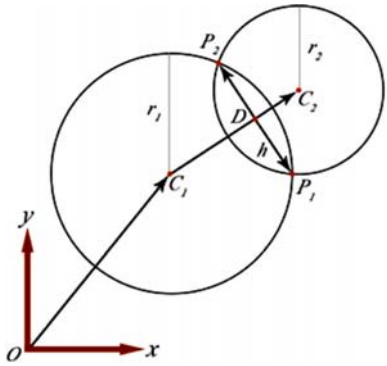

Figure 6. Intersection points of two spheres.

$$l'_{\min} = \max(l_{\min}^{\text{modified}}). \tag{15b}$$

Now, we replace $l_{\max}$ and $l_{\min}$ with $l'_{\max}$ and $l'_{\min}$ in Equation (10) and we have 12 new spheres, 6 spheres for exterior bound and 6 spheres for interior bound. Workspace is defined as intersection between the upper and lower bounds.

To compute the workspace, we discrete the space along the axis z and consider the cross-section of the workspace with planes parallel with plane xy. Therefore, 12 spheres change to 12 circles. Hatching area in Fig. 5 shows a cross-section of workspace.

We cut down each of circles from its intersection points with other circles into the number of arcs. As shown in Fig. 5, the arcs inside all arcs belonging to exterior circles and outside of all arcs belonging to interior circles constitute the boundary of the cross-section of the workspace.

To find the intersections of two circles, we use geometric method that is fast and exact. According to Fig. 6, for points $\mathbf{P}_1$ and $\mathbf{P}_2$, we can write as follows:

$$\mathbf{P}_1 = \overline{\mathbf{OC}_1} + \overline{\mathbf{C}_1\mathbf{D}} + \overline{\mathbf{DP}_1}; \tag{16a}$$

$$\mathbf{P}_2 = \overline{\mathbf{OC}} + \overline{\mathbf{C}_1\mathbf{D}} + \overline{\mathbf{DP}_2}. \tag{16b}$$

Vector $\overline{\mathbf{C}_1\mathbf{D}}$ coincides with vector $\overline{\mathbf{C}_1\mathbf{C}_2}$ and its unit vector is:

$$\hat{\mathbf{C_1D}} = \frac{(x_2 - x_1, y_2 - y_1)}{\sqrt{(x_2 - x_1)^2 + (y_2 - y_1)^2}}. \tag{17}$$

From relation between two triangles $C_1\overset{\Delta}{P}_1D$ and $C_2\overset{\Delta}{P}_1D$, we can write for $\overline{\mathbf{C}_1\mathbf{D}}$:

$$e = |\overline{\mathbf{C}_1\mathbf{D}}| = \frac{r_1^2 - r_2^2 + C^2}{2C}, \tag{18}$$

where C is the distance between centers of circles, $C = |\mathbf{C}_1 - \mathbf{C}_2|$. The unit vectors, which represent the direction of vector $\overline{\mathbf{DP}_1}$ and $\overline{\mathbf{DP}_2}$ are the unit vectors perpendicular to $\overline{\mathbf{C}_1\mathbf{D}}$ and can be written as:

$$\hat{\mathbf{DP}}_1 = -\hat{\mathbf{DP}}_2 = \frac{(y_1 - y_2, x_2 - x_1)}{\sqrt{(x_2 - x_1)^2 + (y_2 - y_1)^2}}. \tag{19}$$

The magnitude of $\overline{\mathbf{DP}_1}$ and $\overline{\mathbf{DP}_2}$ is expressed as:

$$h = |\overline{\mathbf{DP}_1}| = |\overline{\mathbf{DP}_2}| = \sqrt{R_1^2 - |\overline{\mathbf{C}_1\mathbf{D}}|^2}, \tag{20}$$

Hence, Equation (16) becomes:

$$\mathbf{P}_1 = \mathbf{C}_1 + e\,\hat{\mathbf{C}_1\mathbf{D}} + h\,\hat{\mathbf{DP}}_1; \tag{21a}$$

$$\mathbf{P}_2 = \mathbf{C}_1 + e\,\hat{\mathbf{C}_1\mathbf{D}} - h\,\hat{\mathbf{DP}}_1\,. \tag{21b}$$

Having obtained all arcs, now we examine each arc if it belongs to the boundary. Then, we compute the enclosed area by boundary arcs. Gosselin and Angeles [29] proposed an approach to calculate workspace of PMs by Gauss's divergence theorem. Area of surface enclosed with curve ξ is calculated from the following equation:

$$A = \frac{1}{2}\int_{\xi} \mathbf{s}\,\mathbf{n}\mathrm{d}\xi, \tag{22}$$

where $\mathbf{s}$ is the position vector of an arbitrary point of $\mathrm{d}\xi$ and $\mathbf{n}$ is the outward unit normal vector to the curve $\mathrm{d}\xi$.

Consequently, we obtain the area of the cross-section of the workspace for specified z. Repeating this algorithm for all discrete planes, workspace can be written as:

$$\mathrm{ws} = \sum Ad, \tag{23}$$

where d is the distance between discrete planes.

4. Stiffness

For an industrial robot, the stiffness is often one of the main parameters. High stiffness allows operations with high speed. Stiffness S can be expressed as:

$$S = \sqrt{\frac{\Delta\mathbf{p}^T\mathbf{J}^T\mathbf{k}\mathbf{J}\mathbf{J}^T\mathbf{k}\mathbf{J}\Delta\mathbf{p}}{\Delta\mathbf{p}^T\Delta\mathbf{p}}}. \tag{24}$$

where $\Delta\mathbf{p} = [\Delta x, \Delta y, \Delta\psi, \Delta\theta, \Delta\varphi]$ denotes the position and orientation changes of the EE and $\mathbf{k} = \mathrm{diag}[k_1, k_2, \ldots, k_6]$, where k_i is the axial stiffness of limb i.

El-Khasaweh and Ferreira [30] demonstrated that S always falls within two boundaries:

$$\gamma_{\min} < S < \gamma_{\max}, \tag{25}$$

where $\gamma_{\max}$ and $\gamma_{\min}$ are, respectively, minimum and maximum eigenvalues of matrix $\mathbf{J}^T\mathbf{k}\mathbf{J}$.

In many previous works, authors used relation below to define stiffness:

$$k_{\text{ave}} \equiv \sqrt{k_{11}^2 + k_{22}^2 + k_{33}^2}, \tag{26}$$

where k_{ii} are the diagonal elements of the stiffness matrix. However, this index is variant under similarities.

Here, we introduce a new stiffness index invariant under similarities. If v_i represents an eigenvector of matrix $\mathbf{J}^T\mathbf{k}\mathbf{J}$ and γ_i represents the corresponding eigenvalue, stiffness of the manipulator for a given wrench in direction of v_i equals to γ_i [30]. On this basis, we introduce a new stiffness index, geometric mean of eigenvalues (GME):

$$\mathrm{GME} = \frac{\int_{V_{\text{ws}}} k_{\text{gm}}\, \mathrm{d}V_{\text{ws}}}{\int_{V_{\text{ws}}} \mathrm{d}V_{\text{ws}}}, \tag{27}$$

where V_{ws} is the area of the workspace and k_{eig} is:

$$k_{\text{gm}} = \left(\prod_{i=1}^{6} \gamma_i\right)^{1/6}. \tag{28}$$

In other words, k_{gm} is the geometric mean of the stiffness S in direction of eigenvectors of the stiffness matrix. We will show that this stiffness index is invariant under similarities.

6. Particle Swarm Optimization

In this algorithm, we consider a number of particles. The position of each particle in n dimensional space is indicated by one n dimensional vector, where n equals to the number of variables of cost function. Particles move in the space with speed v. The positions and velocities of the particles are updated in each iteration. Criterion of updating the velocity is distance of each particle to local minimums and global minimum computed by Equation (29a). The position of the particles can be calculated from Equation (29b).

$$v_{m,n}^{\text{new}} = v_{m,n}^{\text{old}} + \Gamma_1 \times r_1 \times (p_{m,n}^{\text{local best}} - p_{m,n}^{\text{old}}) + \Gamma_2 \times r_2 \times (p_{m,n}^{\text{global best}} - p_{m,n}^{\text{old}}), \quad (29a)$$

$$p_{m,n}^{\text{new}} = p_{m,n}^{\text{old}} + v_{m,n}^{\text{new}}, \quad (29b)$$

where, $v_{m,n}$ = particle velocity, $p_{m,n}$ = particle position, r_1, r_2 = independent uniform random numbers, $\Gamma_1 = \Gamma_2$ = learning factors = 2, $p_{m,n}^{\text{local best}}$ = best local solution and $p_{m,n}^{\text{global best}}$ = best global solution.

In some respects, PSO is similar to continuous GA but PSO has some advantages over GA. Some previous works compared PSO with other optimization algorithms and showed the advantages of PSO (see, e.g. Ref. [16]). PSO does not require extra operations such as crossover and it has fewer parameters to adjust. In addition, convergence of PSO to optimum region for cost functions, with many variables, is better and faster than GA and constraining the variables in PSO is easier. For these reasons, we choose PSO algorithm to optimize the performance criteria of the 6-DOF PM.

In this paper, we introduce the concept of *random mutation* to develop PSO for our work. The position pattern of the particles after some iteration indicates that particles move toward minimum points and gather around them in clusters. When particles approach to the minimum points, their velocities decrease gradually. For a complicated cost function, with a large number of local minimums, it is possible that all particles are trapped in local minimums. Random mutation moves a percent of the particles to new random positions with new random velocities. It is similar to the mutation operator in GA. We observe that using this method, the algorithm converges to the optimum point rapidly. The flowchart of our algorithm is illustrated in Fig. 7. The number of particles equals 20 and the number of iterations equals 300. Furthermore, we initialize the velocities of the particles in order of 0.1 of the variation ranges of the variables.

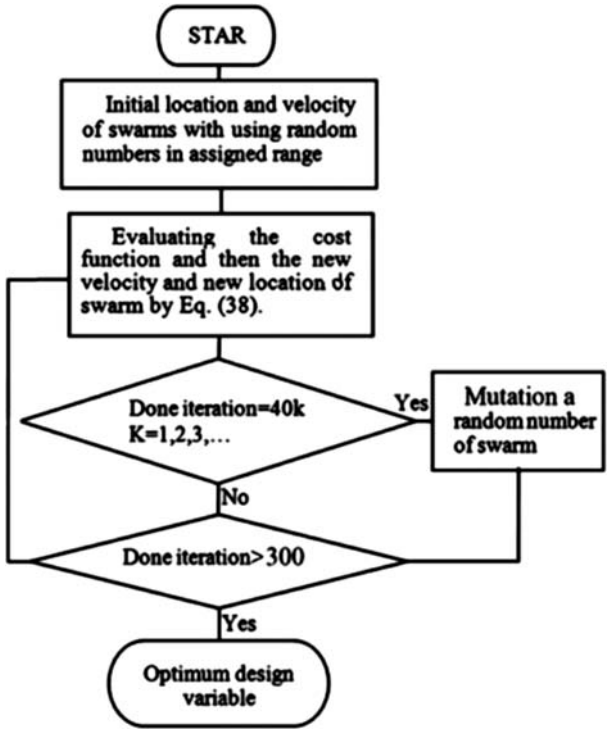

Figure 7. Flowchart of PSO algorithm with random mutation.

7. Results and Discussion

According to Fig. 1, we choose five design variables. These variables specify the geometry of structure clearly. We assigned a constrained variation range to each variable. Design variables and their ranges are presented in Table 1.

Determination of the variation range of the parameters is often difficult when the proposal of a global optimum design is desirable. Therefore, obtaining the optimum similar designs with parameter normalization is an alternative solution.

First, each of parameters R_b, R_p, and Z opts for a value between 0 and 1 and then are normalized:

$$R_{bN} = \frac{R_b}{R_b + R_p + Z}, \tag{30a}$$

$$R_{pN} = \frac{R_p}{R_b + R_p + Z}, \tag{30b}$$

Table 1.
Design variables and their ranges

Variable	Range
R_b	0–1
R_p	0–1
θ_b	0.0873–1.4835 (rad)
θ_p	0.1745–1.0472 (rad)
Z	0–1

$$R_{ZN} = \frac{Z}{R_b + R_p + Z}. \tag{30c}$$

Algorithm executes random mutation after any 40 iterations for 20% of particles selected randomly.

Second, we optimize the workspace and condition number. Third, we try to optimize three parameters together. It is worth noting that trying to optimize workspace and stiffness together leads to a workspace, which is singular at the majority of the points. To optimize the workspace and condition number, we define the cost function as:

$$\text{cost} = -\frac{\text{ws}}{\text{cnd}}, \tag{31}$$

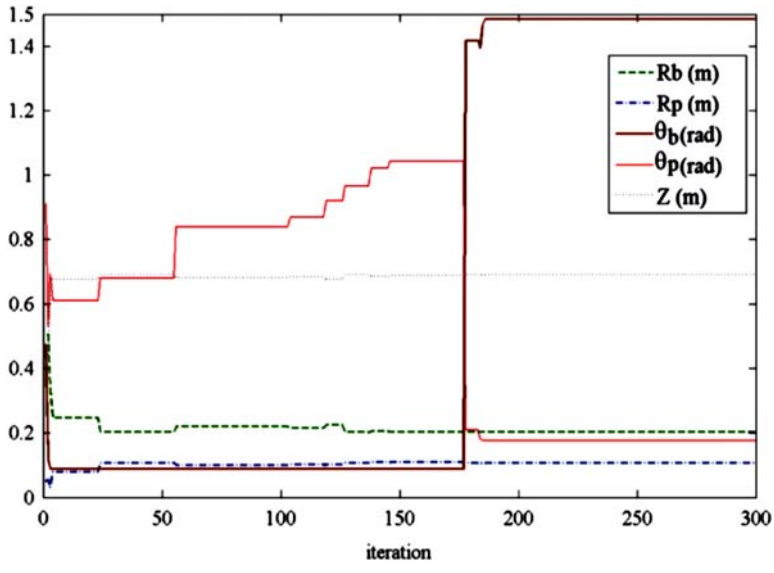

Figure 8. Optimized design variables for workspace and condition number optimization.

where ws represents the workspace and cnd is the condition number, which is calculated from Equation (B2).

Optimization results are shown in Figs. 8 and 9. To compute k_i, we consider constant values for cross-sectional area, A, and the modulus of elasticity, E, for all links. Therefore, the stiffness values in Figs. 9 and 11 must be multiplied by AE to obtain the stiffness in terms of N/m.

Now, we optimize the three parameters including workspace, condition number, and stiffness. For this purpose, we define cost function as:

$$\text{cost} = -\frac{\text{ws} \cdot \text{GME}}{\text{cnd}}. \tag{32}$$

Optimization results are shown in Figs. 10 and 11.

Numerical results are presented in Table 2. For three-parameter optimization, workspace is constrained more and the other parameters reach to better values.

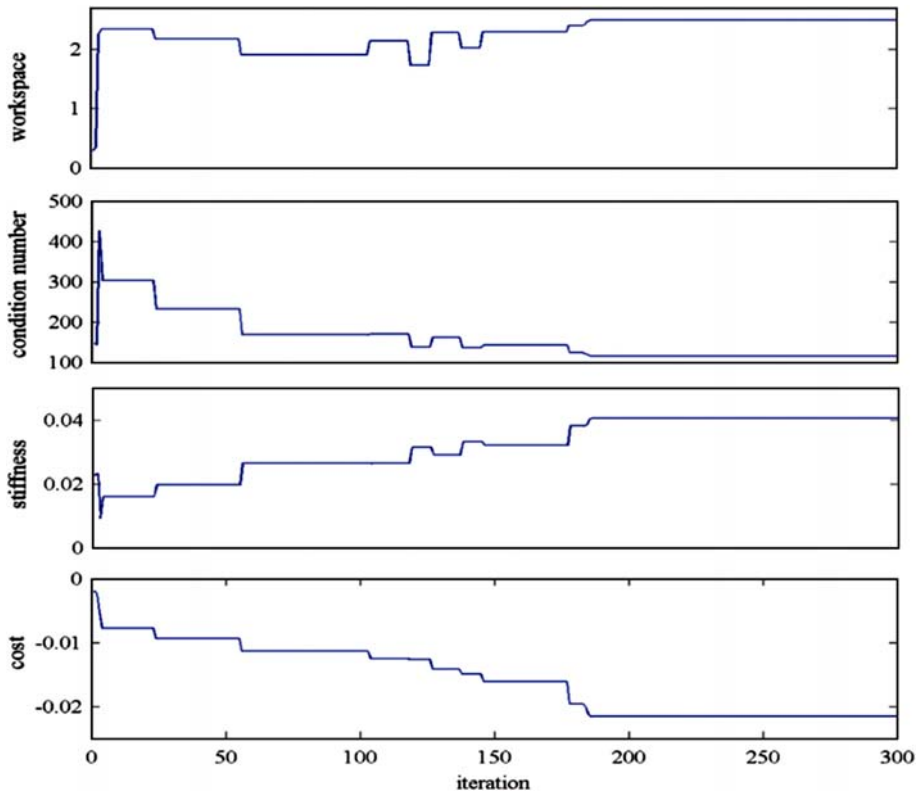

Figure 9. The performance parameters and their total cost function in optimizing workspace and condition number simultaneously.

In all states, the algorithm reaches to stable values after 180 iterations approximately. Therefore, the maximum number of iterations seems to be sufficient.

According to Figs. 8–11, we conclude that the performance parameters highly depend on the variations of Z. Figure 8 suggests that to have an optimum design in two parameter optimization processes, θ_b tends to increase whereas θ_p tends to decrease. Figure 9 reveals that in this optimization procedure, increasing the workspace and decreasing the condition number lead to increase in the stiffness of the PM and decrease in the considered cost function. In addition, as shown in Figs. 8 and 9, the small variations of Z in iterations 120–147 lead to large deviations in the performance parameters. Similar condition can be observed in iterations 120–150 in Figs. 10 and 11. As can be predicted, increasing Z results in increasing the workspace and decreasing the accuracy and stiffness. Moreover, in both of optimization states, as explained partly before, increasing $|\theta_b - \theta_p|$ confines to enhance the performance indices. In three-parameter optimization, the design values R_{b} and R_{p} approach to each other. The maximum difference between the first and second optimizations belongs to R_{p}, which increases 67% in the second one. On the other hand, in the three-parameter optimization, R_{b} and Z decrease 17 and 4%, respectively. Moreover, for the second optimization state, increasing the workspace and condition number and decreasing the stiffness lead to decreasing the desired cost function.

Ultimately, an optimum design for the workspace and condition number is such a design that the radius of the base is twice as many radius of the platform and the height of the structure is approximately 3.5 times more than the radius of the base. For three-parameter optimization, the optimum design is such a

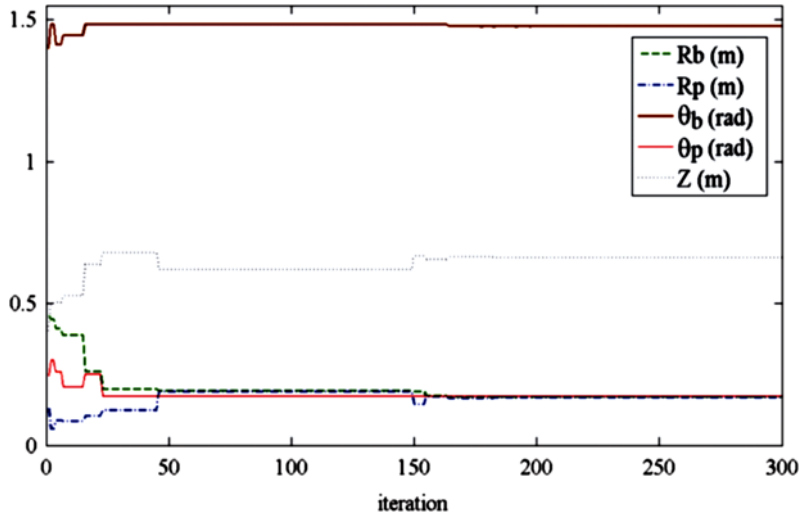

Figure 10. Optimized design variables for optimization of the three performance parameters.

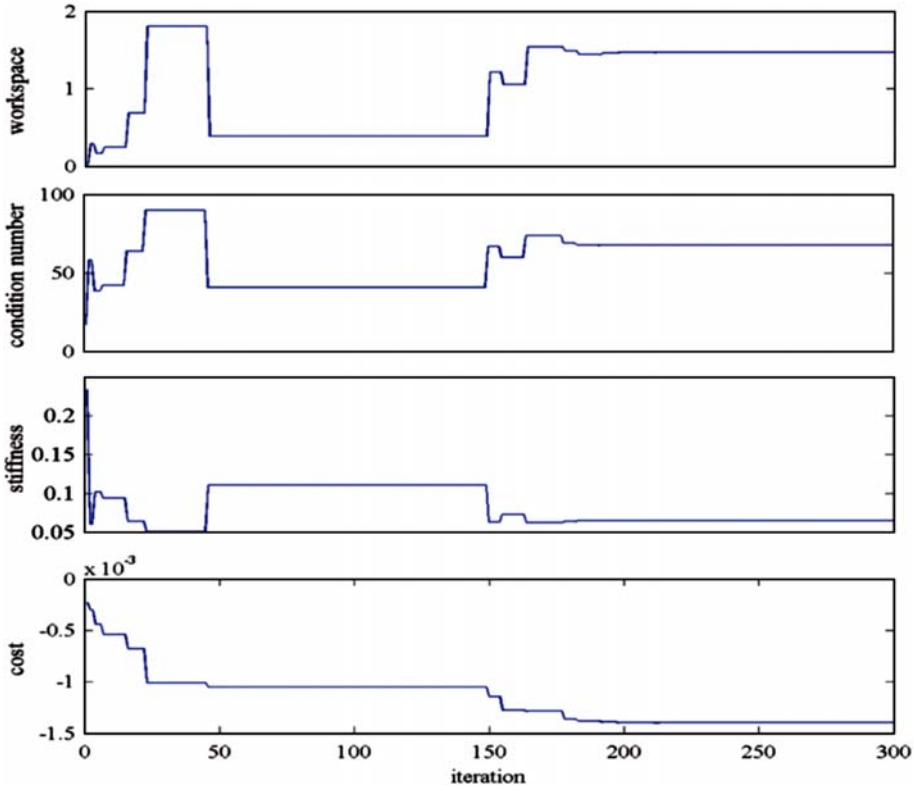

Figure 11. The performance parameters and cost function for optimization of the three performance parameters.

design that the radii of the base and platform are equal which is equal to a quarter of the height. In addition, the links always tend to have maximum tilt.

To verify our results, we compare them with the results presented in Ref. [15]. In that paper, the workspace as one of the most important factors for PMs has not been examined. We use the reported design variables to compare the performance parameters defined in our paper and Ref. [15]. The results are presented in Table 3. As shown in this table, the smaller workspace and larger condition number compared to our results (Table 2) are the weaknesses of the mentioned paper. Of course, they obtained higher stiffness, which can be attributed to the smaller length of the arms. Comparing the results in Table 3 with the results in Table 2, we recognize that our approach improves the workspace and condition number approximately three and two times and in return, the stiffness of the system decreases. The results presented in this paper reveal that there is a good compatibility among three main performance indices including the workspace, condition number, and stiffness.

Table 2.
Optimized parameters

Parameters to optimize	Workspace (m^3)	Condition number	Stiffness (N/m)	R_b (m)	R_p (m)	θ_b (rad)	θ_p (rad)	Z
Workspace and condition number	2.4928	115.39	$0.04054 \times AE$	0.205	0.105	1.4835	0.1760	0.689
Workspace, condition number, and stiffness	1.4675	67.72	$0.06463 \times AE$	0.170	0.169	1.4773	0.1745	0.662

Table 3.
Optimized variables and their performance parameters [15]

Parameters to optimize	Workspace (m^3)	Condition number	Stiffness (N/m)	R_b (m)	R_p (m)	θ_b (rad)	θ_p (rad)	Z
Stiffness and condition number	0.7518	345.21	0.09754 × AE	0.20928	0.1	0.83762	0.31416	0.16064

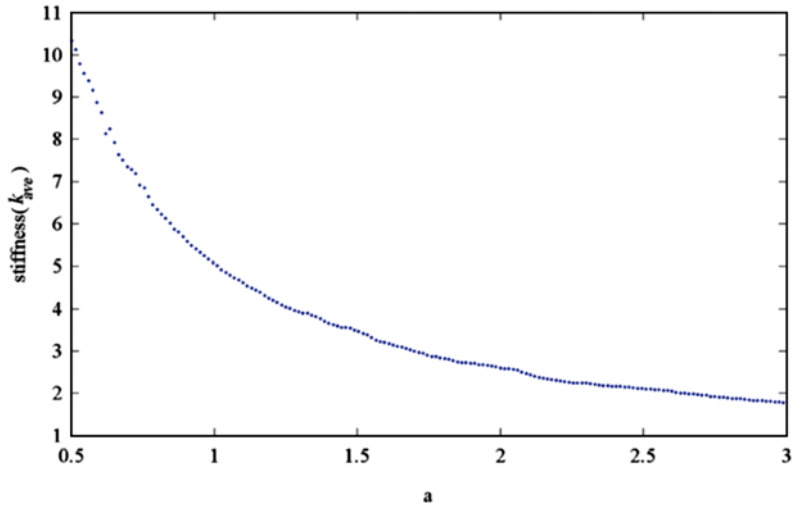

Figure 12. Values of the stiffness when structure is scaled with factor a.

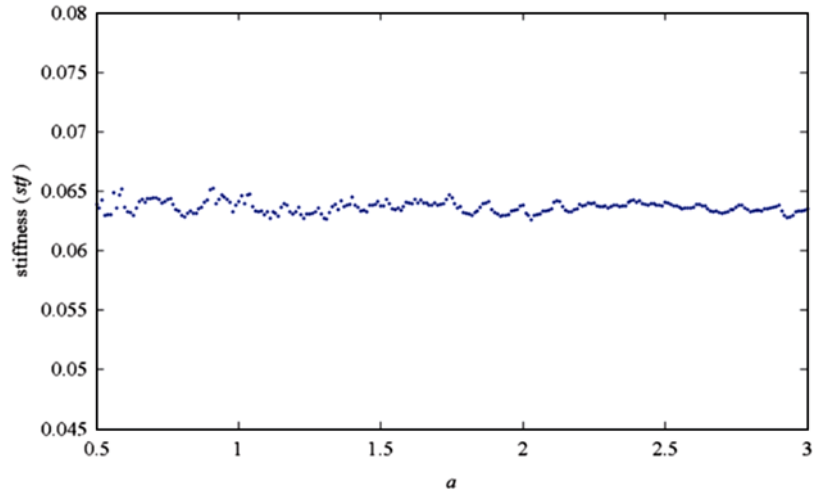

Figure 13. Values of the stiffness index GME when structure is scaled with factor a.

Depending on the fact that which parameter is important for a special case, we can increase its effect in the cost functions by some simple algebraic operators.

We multiplied the parameters R_b, R_p, and Z by scaling factor a when $0.5 < a < 3$ and calculated the stiffness once for performance index k_{ave} and once for performance index GME. The result is shown in Figs. 12 and 13.

One of the main differences of our paper with other previous similar works is that in our stiffness function, all of the values either small or large play central role in optimization process but in the previous works; only key roles are assigned to large numbers in optimization procedure. Our function calculate the small numbers for the reason that the robot may work in their corresponding points and our work leads to more safe designs.

According to Figs. 12 and 13, the stiffness index k_{ave} decrease under similarities, while the stiffness index GME remains constant. Small variations are because of discrete sampling on the workspace.

8. Conclusion

Kinematic analysis of a PM was performed using screw theory. Kim's modified length approach for evaluation of the workspace was explained in more detail in this work. Instead of using the average of diagonal elements of the stiffness matrix, a new performance index was introduced for stiffness estimation. We showed that the new performance index was invariant under similarity. Moreover, we introduced the random mutation in PSO algorithm to improve its convergence and prevent from trapping in local minimums. To reach the optimum similar designs, the three parameters R_b, R_p, and Z were normalized. Then we represented two new cost functions to optimize the workspace, condition number, and stiffness.

The results were compared to two-parameter optimization and it was proved that we could reach a point so that these three parameters situate in acceptable ranges.

The main contributions of this work were simultaneous optimization of three parameters including workspace, stiffness, and condition number and reaching a good compatibility among them as well as introducing the new performance index GME.

References

1. W. M. Craver, Structural analysis and design of a three-degree-of-freedom robotic shoulder module, Master Thesis, The University of Texas at Austin (1989).
2. W. Q. D. Do and D. C. H. Yang, Inverse dynamic analysis and simulation of a platform type of robot, *Int. J. Robotics Syst.* **5**(3), 209–227 (1988).
3. E. F. Fichter, A Stewart platform-based manipulator: general theory and practical construction, *Int. J. Robotics Res.* **5**(2), 157–182 (1986).

4. C. Gosselin and J. Angeles, The optimum kinematic design of a planar three-degree-of-freedom parallel manipulator, *ASME J. Mech., Trans., Automat. Des.* **110**(1), 35–41 (1988).
5. K. M. Lee and D. K. Shah, Dynamic analysis of a three-degree-of-freedom in-parallel actuated manipulator, *IEEE J. Robotics Automat.* **4**(3), 361–367 (1988).
6. J. A. Carretero, M. Nahon, C. M. Gosselin and B. Buckham, Kinematic analysis of a three-DOF parallel mechanism for telescope applications, in: *Proc. 1997 ASME Design Automation Conference, Sacramento*, Paper No. DETC97/DAC-3981 (1997).
7. C. Hua, C. Weishan and L. Junkao, Optimal design of Stewart platform safety mechanism, *Chinese J. Aeronaut.* **4**(20), 370–377 (2007).
8. F. Majou, P. Wenger and D. Chablat, Design of a 3-axis parallel machine tool for high speed machining: the orthoglide, in: *Proc. 4th Int. Conf. on Integrated Design and Manufacturing in Mechanical Engineering*, Clermont-Ferrand, pp. 1–10 (2002).
9. H. S. Kim and L.-W. Tsai, Design optimization of a Cartesian parallel manipulator, *ASME J. Mech. Des.* **125**(1), 43–51 (2003).
10. F. Hao and J.-P. Merlet, Multicriteria optimal design of parallel manipulators based on interval analysis, *Mech. Mach. Theory* **40**(2), 157–171 (2005).
11. Y. Lou, D. Zhang and Z. Li, Optimal design of a parallel machine based on multiple criteria, in: *Proc. IEEE Int. Conf. on Robotics and Automation*, Barcelona, pp. 3219–3224 (2005).
12. B. Monsarrat and C. M. Gosselin, Workspace analysis and optimal design of a 3-leg 6-DOF parallel platform mechanism, *IEEE Trans. Robotics Automat.* **19**(6), 954–966 (2003).
13. M. Badescu and C. Mavroidis, Workspace optimization of 3-legged UPU and UPS parallel platforms with joint constraints, *ASME J. Mech. Des.* **126**(2), 291–300 (2004).
14. Y. K. Hwang, J. W. Yoon, Christiand, J. H. Ryu, The optimum design of a 6-DOF parallel manipulator with large orientation workspace, in: *Proc. IEEE Int. Conf. on Robotics and Automation*, Roma, pp. 1255–1259 (2007).
15. Z. Gao, D. Zhang and Y. Ge, Design optimization of a spatial six degree-of-freedom parallel manipulator based on artificial intelligence approaches, *J. Robot. Computer-Integrated Manuf.* **26**(2), 180–189 (2009).
16. Q. Xu and Y. Li, Error analysis and optimal design of a class of translational parallel kinematic machine using particle swarm optimization, *J. Robotica* **27**, 67–78 (2009).
17. J. Kennedy, R. C. Eberhart, Particle swarm optimization, in: *Proc. IEEE Conf. on Neural Networks*, Perth, pp. 1942–1948 (1995).
18. C. Trelea, The particle swarm optimization algorithm: convergence analysis and parameter selection, *Inform. Process. Lett.* **85**(6), 317–325 (2003).
19. M. Jiang, Y. P. Luo and S. Y. Yang, Stochastic convergence analysis and parameter selection of the standard particle swarm optimization algorithm, *Inform. Process. Lett.* **102**(1), 8–16 (2007).
20. Z. Zhan and J. Zhang, Adaptive particle swarm optimization, *Lecture Notes in Computer Science*. Springer, Berlin. pp. 227–234 (2008).
21. T. H. Davies, Kirchhoff's circulation law applied to multi-loop kinematic chains, *Mech. Mach. Theory* **16**(3), 171–183 (1981).
22. M. G. Mohamed and J. Duffy, A direct determination of the instantaneous kinematics of fully parallel robot manipulators, *ASME J. Mech., Trans., Automat. Des.* **107**(2), 226–229 (1985).
23. K. Sugimoto, Kinematic and dynamic analysis of parallel manipulators by means of motor algebra, *ASME J. Mech., Trans., Automat. Des.* **109**(1), 3–5 (1987).
24. V. Kumar, Instantaneous kinematics of parallel-chain robotic mechanisms, *ASME J. Mech. Des.* **114**(3), 349–358 (1992).

25. I. A. Bonev and J. Ryu, A new approach to orientation workspace analysis of 6-DOF parallel manipulators, *Mech. Mach. Theory* **36**(1), 15–28 (2001).
26. J. S. Zhao, M. Chen, K. Zhou, J. X. Dong and Z. J. Feng, Workspace of parallel manipulators with symmetric identical kinematic chains, *Mech. Mach. Theory* **41**(6), 632–645 (2006).
27. C. Gosselin, Determination of the workspace of 6-DOF parallel manipulators, *ASME J. Mech. Des.* **112**(3), 331–336 (1990).
28. D. I. Kim, W. K. Chungt and Y. Youmt, Geometrical approach for the workspace of 6-DOF parallel manipulators, in: *Proc. IEEE Int. Conf. on Robotics and Automation*, New Mexico, pp. 2986–2991 (1997).
29. C. Gosselin and J. Angeles, The optimum kinematic design of a planar three-degree-of-freedom parallel manipulator, *ASME J. Mech., Trans., Automat. Des.* **110**(1), 35–41 (1988).
30. B. S. El-Khasawneh and P. M. Ferreira, Computation of stiffness and stiffness bounds for parallel link manipulators, *J. Mach. Tools & Manuf.* **39**(2), 321–342 (1999).
31. R. S. Ball, *The Theory of Screws*. Cambridge University Press, Cambridge (1900).
32. K. J. Waldron, The constraint analysis of mechanisms, *J. Mech.* **1**(2), 101–114 (1966).
33. K. H. Hunt, *Kinematic Geometry of Mechanisms*. Clarendon Press, Oxford (1978).
34. J. P. Merlet, *Parallel Robots*, 2nd ed. Springer, Dordrecht, the Netherlands (2006).

Appendix A. Screw Theory

Mathematical bases of this method were established by Ball [31] and then its applications in analytic mechanics were developed by some researchers such as Waldron [32] and Hunt [33]. However, for the first time, Mohamed and Duffy [22] used screw theory to compute the Jacobian matrix of a PM. The structure under discussion in this paper is depicted in Fig. 1 which is a UPS-6DOF PM. It is also known as Gough–Stewart platform.

We assign one screw to each joint. Each screw is a vector with six components. For revolution joints, the screw is defined as:

$$\hat{\$} = \begin{bmatrix} \mathbf{s} \\ \mathbf{s_0} \times \mathbf{s} \end{bmatrix}. \tag{A1}$$

and the screw of prismatic joints is given by:

$$\hat{\$} = \begin{bmatrix} \mathbf{0} \\ \mathbf{s} \end{bmatrix}, \tag{A2}$$

Where $\mathbf{s}$ is the vector that represents the orientation of axis of the joint and $\mathbf{s_0}$ is a position vector of an arbitrary point on the axis of the joint.

The relation between twist of the EE and the velocities of the joints, including active and passive joints, is represented by:

$$\sum_{n=1}^{6} \dot{\theta}_{n,i} \hat{\$}_{n,i} = \mathbf{S_t}, \quad 1 \leqslant i \leqslant 6, \tag{A3}$$

where $\mathbf{S_t}$ represents the twist of the EE, $\hat{\$}_{n,i}$ and $\dot{\theta}_{n,i}$ represent, respectively, screw and velocity of nth joint of the ith limb. However, we want to obtain the relation between twist of the EE and active joints. Therefore, we should find the *reciprocal screws*. Reciprocal screw of $\$$ is $\$^T$, if the following equation is satisfied:

$$\Omega(\$, \$^T) = 0, \tag{A4}$$

where $\Omega(\$, \$^T)$ is defined as:

$$\Omega(\$, \$^T) \equiv \$_1\$_4 + \$_2\$_5 + \$_3\$_6 + \$_4\$_1 + \$_5\$_2 + \$_6\$_3. \tag{A5}$$

For a given chain with one active joint, the reciprocal screw is one that the result of its multiplying by all joint screws is zero except active joint. With multiplying the reciprocal screw in Equation (A3), we find the Jacobian matrix (for more details, see Refs [25,31–33]).

Appendix B. Condition Number

Condition number has been recognized as a main parameter of the robots to indicate their accuracy. In other words, condition number expresses the magnification ratio of the error produces in joints and equals to [34]:

$$\kappa(\mathbf{J}) = \|\mathbf{J}\| \cdot \|\mathbf{J}^{-1}\|, \tag{B1}$$

where $\|.\|$ represents norm. Two norms that are mostly used are Euclidean norm and 2-norm. Owning to the fact that computing Euclidian norm is a time-consuming process, we use 2-norm. Therefore, condition number equals to the ratio of maximum and minimum eigenvalues of matrix $\mathbf{J}^T\mathbf{J}^{-1}$.

Condition number varies between 1 and ∞. At singular point, the condition number is infinite. Manipulator designers are interested in reducing the condition number as far as possible. We evaluate the average condition number at the discrete points on the whole area of the workspace which is defined as:

$$\text{cnd} = \frac{\int_{V_{\text{ws}}} \kappa \, \mathrm{d}V_{\text{ws}}}{\int_{V_{\text{ws}}} \mathrm{d}V_{\text{ws}}}. \tag{B2}$$

About the Authors

Ataollah Ramezan Shirazi received the BS degree in Solid State Physics from University of Tehran, Tehran, Iran, in 2008, and the MS degree in Mechatronics Engineering from University of Tabriz, Tabriz, Iran, in 2010. Since 2010, he has been an industrial automation engineer at mechatronics laboratory of Automobile Technology Industrial Park, Tabriz, Iran. His research interests include mechatronics, robotics, artificial intelligent, control, and machine vision.

Mir Masoud Seyyed Fakhrabadi received his BS and MS in mechanical engineering from the University of Tabriz, Tabriz, Iran, in 2007 and 2009, respectively, both of them with honors. He is currently a PhD candidate of nanomechnics engineering at the University of Tehran, Tehran, Iran, and a research assistant with the Mechatronics Research Laboratory, University of Tabriz. His research interests include nanomechanics, dynamics and control of MEMS and NEMS, robotics and mechatronics and application of artificial intelligence in engineering problems. He is the author of more than 50 journals and conference papers related to these fields. Also, he has seven books in mathematics and mechanical engineering fields. He was honored several times by different organizations such as Iran's ministry of science, research and technology as an outstanding and distinguished student among more than 3,500,000 Iranian students. Also, he is a member of Iran's national elite's organization and exceptional talents offices at the University of Tehran and University of Tabriz. He has been the referee of several journal and conference papers including ASME and IEEE conferences.

Ahmad Ghanbari received the BS and MS degrees in mechanical engineering from California Polytechnic State University, Pomona, California, in 1978 and 1980 respectively. He received the PhD degree of electrical engineering from the University of Tabriz, Tabriz, Iran in 2007. He is currently an associate professor with the department of mechanical engineering and school of engineering-emerging technologies, University of Tabriz. His research interests include mechatronics, dynamics, control, robotics and artificial intelligence. He is author of about 40 journal and conference papers related to these fields. He is a member of ASME, Iranian Society of mechanical engineering (ISME) and Iranian Society of Mechatronics. Also, he is the director of Center of Excellence for Mechatronics at the University of Tabriz.